

pubs.acs.org/JACS Article

Elucidating the Roles of Local and Nonlocal Rate Enhancement Mechanisms in Plasmonic Catalysis

Rachel C. Elias and Suljo Linic*



Cite This: J. Am. Chem. Soc. 2022, 144, 19990-19998



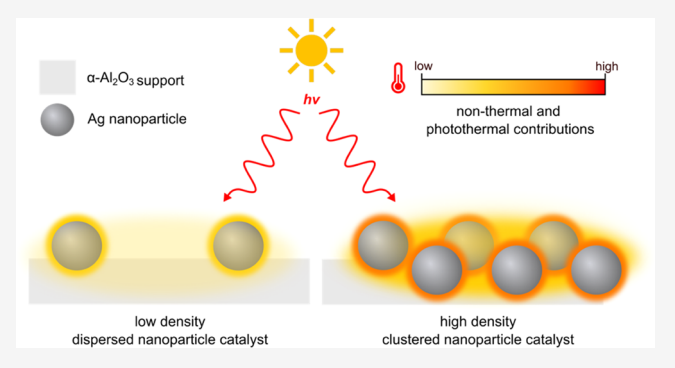
ACCESS I

III Metrics & More

Article Recommendations

SI Supporting Information

ABSTRACT: Plasmonic metal nanoparticles (e.g., Ag, Au, and Cu) constitute a class of materials that interact with light via the excitation of localized surface plasmon resonance (LSPR). Numerous studies have reported substantial enhancements in the rates of chemical reactions on illuminated plasmonic nanoparticle catalysts compared to corresponding systems in the absence of illumination. There are two mechanisms that have been proposed to explain the LSPR-induced chemical reactivity. One mechanism assumes a local plasmon-induced hot charge-carrier-mediated activation of the reactants, while the other assumes an LSPR-induced equilibrium heating of the catalyst, which leads to energy transfer to and chemical reaction of the adsorbed reactants. In this



contribution, we developed a setup amenable to accurate in situ catalyst temperature and kinetic reaction rate measurements. We employed this setup to study the LSPR-induced rate enhancement in a case study of the CO oxidation reaction on plasmonic, monometallic Ag nanoparticle catalysts supported on α -Al₂O₃. We explored various Ag loadings and clustering levels. Our data show that the equilibrium heating of the catalyst cannot fully explain the illumination-induced plasmonic rate enhancements. This is the case even for high loading and clustering of Ag nanoparticles, where the equilibrium heating significantly increases. Based on the analysis, we propose that local effects, related to the plasmon-induced activation of adsorbates (reactants) via electronic excitation of the reactant or photothermal heating of the reactants that is highly localized to the individual nanoparticles, play a critical role in driving LSPR-induced chemical reactions.

■ INTRODUCTION

Plasmonic metal nanoparticles (e.g., Ag, Au, and Cu) represent a class of materials that interact strongly with light via localized surface plasmon resonance (LSPR) excitation. LSPR is characterized by large optical extinction cross sections of the plasmonic metal nanoparticles and the generation of elevated electric fields, mainly confined to their surfaces. Over the past decade, it has been well established that under conditions of LSPR, these nanomaterials can activate photocatalytic reactions due to their ability to harvest and redirect the supplied light energy to drive chemistry on their surfaces. Numerous studies have reported substantial reaction rate enhancements on illuminated plasmonic nanoparticle catalysts compared to corresponding rates under nonilluminated conditions.

There is an interest to understand and quantify the mechanisms responsible for the observed plasmon-induced reaction rate enhancements. In general, the fundamental outstanding questions are related to the mechanisms and pathways by which light energy moves through a plasmonic catalytic system to induce chemical reactivity. For chemical reactions to take place, the reactant must be heated (i.e., its vibrational states excited). We note that here we are referring to nonredox gas-phase thermal reactions and not to electron-

transfer electrochemically driven reactions. In a plasmonic system, this can occur via selective heating of the reactant as hot charge carriers (electrons or holes that are not thermalized), produced in the decay of LSPR, scatter through the molecule via the hot charge-carrier mechanism. This scattering of nonthermalized, energetic charge carriers through adsorbates can lead to vibrational heating and chemical transformation of the adsorbates, without the equilibrium heating of the catalyst. 18,19 We note that the scattering of the nonthermalized hot charge carriers through an adsorbate can take place via excitation of charge carriers in the nanoparticle and their ballistic transfer to the adsorbate or via the direct excitation of energetic charge carriers at the nanoparticleadsorbate interface.²⁹ Alternatively, the reactants can be heated as energy is transferred from the catalyst phonon modes to the reactant vibrational modes via the photothermal heating

Received: August 11, 2022 Published: October 24, 2022





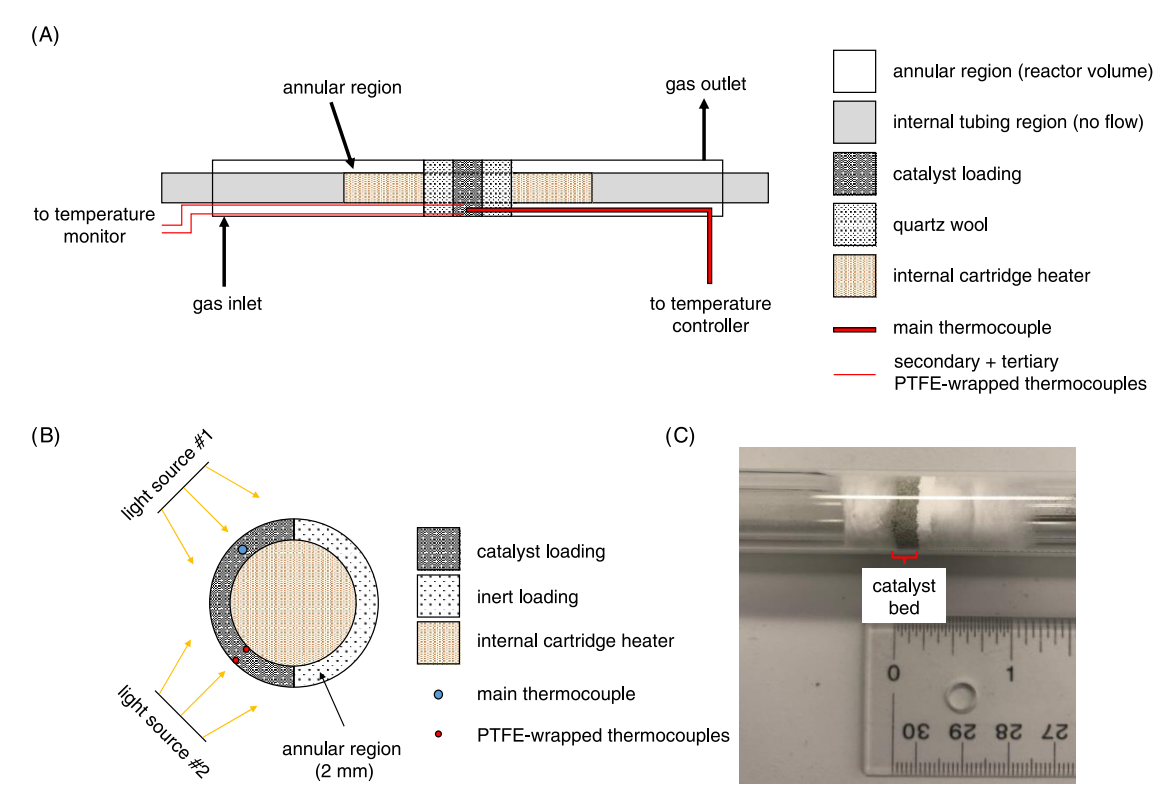
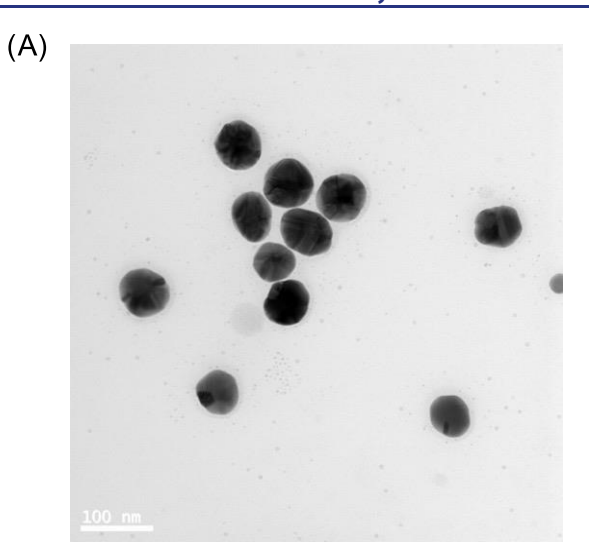


Figure 1. Annular reactor design. (A) Side view of the reactor showing the reactor inlet and outlet locations as well as the positioning of the thermocouples within the catalyst bed; (B) top-down view of the reactor, showing the catalyst loading configuration, with half of the annular region loaded with the active material and the other half of the annular region loaded with an inactive material of identical particle size (here, α -Al₂O₃); and (C) photograph of a sample reactor loading; the image shows the half of the reactor loaded with the active catalyst material.

mechanism.³⁰ In this mechanism, the decay of LSPR leads to excited charge carriers within the nanoparticle, which are thermalized with the phonon modes of the nanoparticle and its surroundings before they scatter through the adsorbates, resulting in equilibrium catalyst heating that yields enhanced reaction rates. The practical difference between these two mechanisms is that while charge-carrier-driven processes may modify the reaction pathway, photothermal heating should act only by increasing the effective temperature of the catalytic system, and therefore the reaction selectivity should not be affected.³¹

In principle, if the photothermal mechanism dominates, then by measuring the temperature of the catalyst under illumination (due to the equilibration of the system temperature, the reactant is at the same temperature as the catalyst), we should be able to account for the LSPR-induced increases in reaction rate. On the other hand, if the hot charge-carrier mechanism plays a role, then the LSPR-induced changes in the catalyst temperature should not be able to completely account for the changes in the reaction rate. While evidence in the form of kinetic isotope studies, unique reaction product selectivity under illumination, and other phenomena have suggested that energetic charge carriers often play an important role in the enhancement mechanism, 9,10,14,29,32 few works have attempted to rigorously quantify and isolate nonthermal and photothermal contributions in the functioning catalysts, where plasmonic nanoparticles are packed in three-dimensional macroscopic reactor beds. 24,33

A significant challenge in quantifying the relative importance of the different LSPR-induced rate enhancement mechanisms, in part, lies in the inherent difficulties in measuring equilibrium photothermal heating under illumination in these catalysts. 28,34 Accurately measuring the temperature of a catalyst under illumination is not trivial since the catalyst is usually packed in a three-dimensional bed that is most often illuminated from one side, inducing significant light-induced temperature gradients in the bed. To measure the temperature of the catalyst bed, either a thermocouple or infrared (IR) camera is typically employed, ^{28,34} and both techniques pose some risk for inaccuracies.³⁵ For instance, in the case of infrared measurements, it is necessary to have a reliable understanding of the catalyst's emissivity to obtain accurate surface temperature measurements. Unfortunately, due to the strong light-matter interactions that are highly sensitive to the catalyst (nanoparticle) geometry and concentration, it is difficult to accurately assess the emissivity of plasmonic nanoparticles packed in a three-dimensional catalyst bed. Furthermore, since IR cameras mainly probe the surface temperature of the catalyst—the region typically most impacted by illuminationthese measurements are better suited for two-dimensional systems and may overestimate the average temperature in a three-dimensional catalyst bed. Measurements relying on thermocouples can also overestimate the temperature of the catalyst bed, as many thermocouples respond to light illumination by temperature changes due to the optical excitations within the thermocouple materials. This is especially problematic when the thermocouple is not fully embedded in the catalyst layer and is exposed more directly to the light source. For instance, we found that directly illuminating an OMEGA stainless steel sheathed K-type thermocouple (the same thermocouple we use in our catalyst temperature measurements) using a broadband visible light



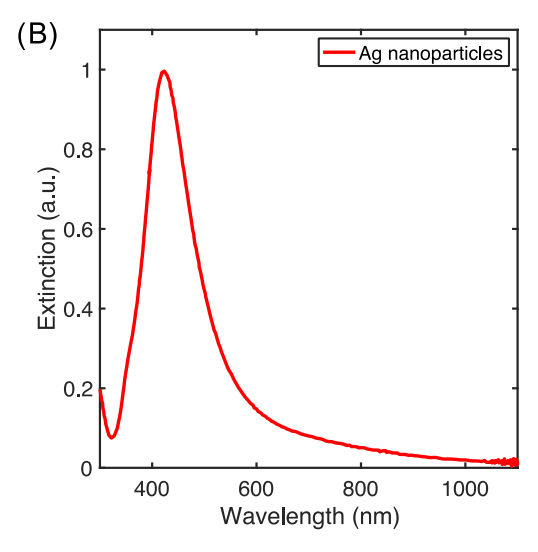


Figure 2. Characterization of Ag nanoparticle catalysts. (A) Bright-field STEM image of the nanoparticles shows the formation of spheres with an average diameter of 64 nm; (B) UV—vis extinction spectrum of Ag particles dispersed in water shows the plasmon peak around 420 nm, consistent with Ag nanospheres of this size.

source with its peak intensity at 400 mW/cm² can lead to artificially inflated measured temperature by tens of degrees. We found that for accurate measurements, it is critical to wrap the thermocouple with light-reflective materials, as described in the Experimental Section. For a more in-depth discussion of the limitations of these approaches, we direct the reader to a few recent review articles, which explore these issues of experimental technique in comprehensive detail.^{28,34}

Another issue in designing meaningful experiments where the temperature of the catalyst can be correlated to the reaction rates is that the measurements must be performed in the so-called kinetic regime, where the measured rates are not controlled by the mass transport of reactants to the reactive catalyst surface. In general, this requires reactor systems where the rate of mass transport to the active catalytic sites can be controlled. In addition, it is desired to have a catalyst bed that is not overly thick or thin, so that at least a large fraction of the bed is interacting with light and that, at the same time, a large fraction of light does not penetrate through the reactor without interacting with the catalyst. ^{24,33,35,36}

To develop a setup amenable to accurate in situ catalyst temperature and kinetic reaction rate measurements, we designed and built an annular quartz tube photoreactor that addresses the above-mentioned issues and deficiencies that have hampered previously employed commercial reactors. ^{8,9,19,37} We employed this reactor to study the rate enhancement for the CO oxidation reaction over plasmonic, monometallic Ag nanoparticle catalysts supported on α -Al₂O₃. We explored the effect of the Ag nanoparticle density and clustering on equilibrium photothermal heating by comparing plasmonic rate enhancements across a range of catalyst loadings of 1.5, 3, 6, and 12 wt % Ag on α -Al₂O₃ (the percentage loading of Ag nanoparticles in the catalyst bed by weight). Our findings suggest that the equilibrium heating of the catalyst bed cannot account for the magnitude of the reaction rates observed for the illuminated catalyst bed. This is the case even for high loading and clustering of Ag nanoparticles, where equilibrium heating increases significantly. Our analysis suggests that local processes—including plasmon-induced activation of adsorbates (reactants) via their electronic excitation or heating of these adsorbates that

remains highly localized to the individual nanoparticles—are the drivers of the measured LSPR-induced chemical reactivity.

EXPERIMENTAL SECTION

The annular quartz reactor consisted of two tubes of different radii oriented coaxially. The design of the reactor (Figure 1) was aided by fluid flow simulations performed with COMSOL Multiphysics software, which was employed to solve the governing fluid flow equations. This allowed us to assess the utility of the reactor in measuring meaningful reaction rates. In short, the simulations were used to understand the residence time distribution and flow patterns in an annular reactor to ensure that under operating conditions the reactor geometry allowed for the plug flow conditions required to accurately measure kinetic rates. The supporting of the model setup are provided in the Supporting Information.

Ag nanoparticles of spherical shape $\sim\!60$ nm in diameter were synthesized using a previously described polyol method. $^{39-41}$ The Ag nanoparticle catalysts were supported on a mechanically stable, optically and chemically inert, low-surface-area α -Al₂O₃ support at different Ag weight loadings using a method previously reported. ¹⁷ Further details of nanoparticle and catalyst preparation and characterization are available below in the text and in the Supporting Information.

The photoreactor design, shown in Figure 1, provided an annular region of 2 mm thickness. The catalyst was loaded into the reactor, which we operated in a vertical configuration. The reactor was heated from the interior of the reactor using a cartridge heater positioned in direct contact with the internal quartz tube. The temperature of the catalyst bed within the reactor was monitored using a thin stainless steel sheathed thermocouple embedded directly within the catalyst. We loaded half of the annular region in the azimuthal direction with the catalyst and the other half was loaded with an inert α -Al₂O₃ of equivalent particle diameter (Figure 1b). For photothermal operation, the catalyst-loaded portion of the annular photoreactor was illuminated externally using two adjacent Dolan-Jenner Fiberlite 180 light sources, both equipped with IR cutoff filters. The peak intensity of the light was measured to be ~400 mW/cm² at the inside surface of the exterior tube (i.e., where the catalyst sits), and the wavelength profile of the light source (spanning from ~200 to 800 nm) is provided in the Supporting Information. When obtaining photothermal rate data, the temperature control system was maintained at a constant heater power, i.e., the feedback mechanism was disabled so that the power supplied to the cartridge was constant in each given set of thermal and photothermal measurements. This allowed us to compare thermal and photothermal rates at a constant

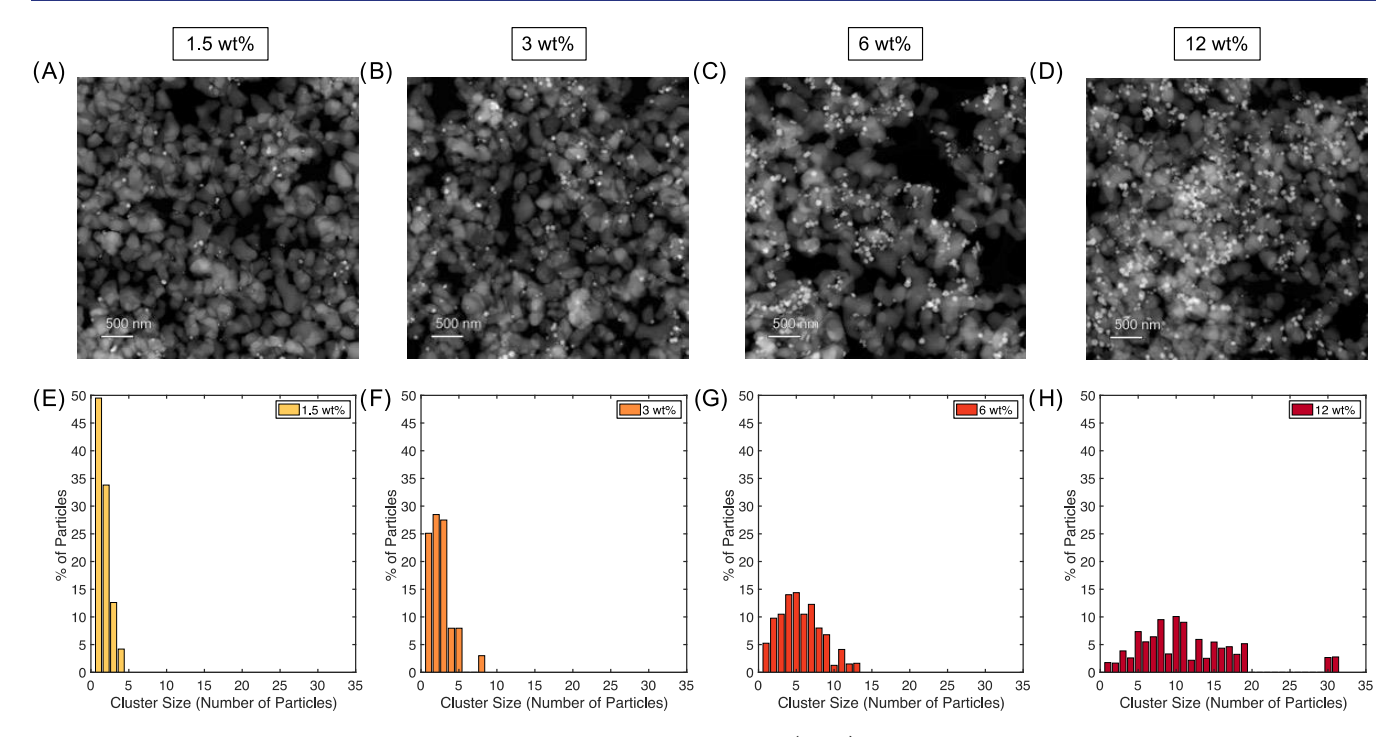


Figure 3. Imaging and quantification of Ag particle clustering on α -Al₂O₃ support. (A–D) High-angle annular dark-field images of Ag nanoparticle catalysts of 1.5, 3, 6, and 12 wt % Ag loading deposited on the α -Al₂O₃ support; (E–H) corresponding nanoparticle clustering distribution for each catalyst loading, suggesting that only at high loadings does large Ag cluster formation (>10 particles per 0.15 μ m²) become prevalent.

external heater temperature. Chemically and optically inert quartz wool was used to keep the catalyst bed in place, ensure a uniform bed thickness, and prevent channeling or other flow irregularities. The catalyst layer was typically measured to be between 4 and 5 mm in length.

To measure the temperature within the catalyst at different positions, thermocouples were embedded in the catalyst bed. The thermocouples were wrapped in several layers of PTFE sealant tape to minimize artificial temperature increases measured when light impinges directly on the thermocouple. Through a few control experiments detailed in the Supporting Information, we found that wrapping the thermocouple with PTFE tape reduced the measured temperature increase under illumination, which we attribute to the direct light-induced heating (or even electronic excitations) of the stainless steel thermocouple sheath. As described in the Supporting Information, even with these precautions, it is likely that our photothermal catalyst temperature measurements, particularly at the point in the reactor closest to the light source, may still slightly overestimate the true macroscopic steady-state temperature by no more than 5 or 6°.

We studied CO oxidation as a probe reaction. The experiments were conducted at 100 sccm and 5% CO and 5% $\rm O_2$, with a balance of nitrogen. Reaction data were collected under a kinetically limited regime at conversions typically below 5%, which was maintained by keeping our weight hourly space velocity relatively high. We note that this excludes just two data points where the plasmonic enhancements pushed the reaction conversion to values higher than 5%. Reaction products were examined using gas chromatography (Agilent 7890B). More details regarding conversion for each catalyst are provided in the Supporting Information.

All catalysts were pretreated by calcination at 200 °C in 20% O_2 , balance N_2 for 3 h to burn off residual organic stabilizer, and were subsequently reduced at 200 °C in 20% H_2 , balance N_2 to reverse any surface oxidation imposed during the calcination step. Afterward, the catalyst was subjected to the initial reaction conditions and allowed to reach steady-state overnight (typically 12 h) before collecting reaction rate data. The reactor was operated at atmospheric pressure.

RESULTS AND DISCUSSION

Figure 2a shows as-synthesized Ag nanoparticles imaged using bright-field scanning transmission electron microscopy (STEM). The image shows that Ag nanoparticles are spherical with an average diameter of 64 \pm 9.5 nm. 41 Figure 2b shows the UV–vis extinction spectrum of the nanoparticles suspended in water, demonstrating a plasmon resonance near 420 nm. As described above, these Ag nanoparticles were supported on α -Al₂O₃. Figure 3a–d shows the representative high-angle annular dark-field (HAADF) STEM images of the Ag/ α -Al₂O₃ catalysts with 1.5, 3, 6, and 12 wt % Ag nanoparticle loadings.

A visual inspection of the STEM images in Figure 3 reveals that higher-loaded catalysts exhibited not only a higher average particle density but also a higher propensity for particles to aggregate and cluster. To confirm this qualitative observation, we developed a procedure to quantify the extent of nanoparticle clustering via an imaging analysis approach using ImageJ and MATLAB. We analyzed multiple representative images from each catalyst sample and calculated the percentage of nanoparticles for each weight loading that was found in clusters of different sizes. The detailed approach is provided in the Supporting Information. Briefly, each STEM image was divided into 16 equally spaced rows and columns to yield 256 smaller "tiled" images of the identical area (each tile corresponding to a 0.15 μ m² region). The number of particles residing in each tile was counted. Technically speaking, based on the dimensions of the tiles, any two or more particles separated by ~387 nm or less were considered members of the same cluster. However, we found that the particles determined to reside within the same cluster were typically very close neighbors, separated by less than 10 nm. This was especially true for higher-loaded catalysts. We found that while nearly all nanoparticles in the 1.5 and 3 wt % catalysts were isolated or in very small clusters of 2-5 nanoparticles, clustering was very

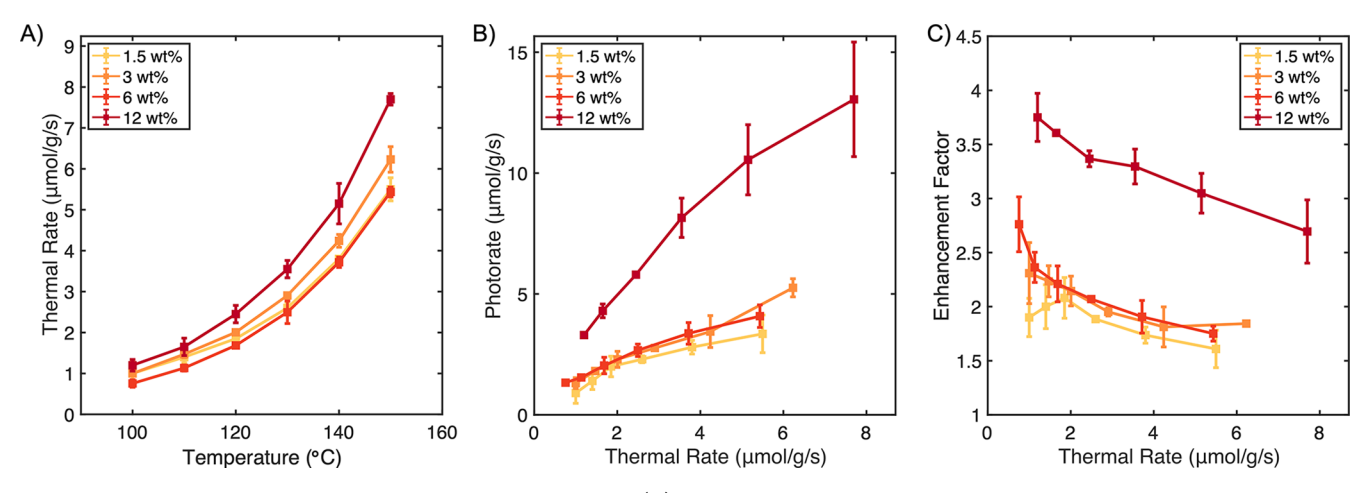


Figure 4. Measured rates of CO oxidation on Ag/α - Al_2O_3 catalysts. (A) Thermal rate data for the CO oxidation reaction on 1.5, 3, 6, and 12 wt % Ag/α - Al_2O_3 catalysts demonstrate similar rates per gram of catalyst for each loading, consistent with operation in a kinetically limited regime; (B) photorates for each catalyst loading between 1.5 and 6 wt % remain similar, suggesting the absence of loading-dependent collective effects at these low to moderate loadings; for the 12 wt % catalyst, the photorates increase substantially, suggesting the increase of collective effects; and (C) enhancement factors for each catalyst loading calculated by dividing the photothermal rates by respective thermal rates measured under identical external heat supply; all error bars represent the standard deviation for data collected from multiple reactor loadings.

prominent in 12 wt % catalysts. The distributions of the number of nanoparticles in clusters as a function of cluster size for each catalyst loading are shown in Figure 3e—h. We also analyzed our catalyst postreaction to confirm that the morphology of individual nanoparticles and clusters did not change significantly over the course of the reaction studies. Additional STEM images confirming an absence of significant morphological changes to the catalyst are provided in the Supporting Information. We attribute this catalyst stability to the mild operating conditions (temperatures and pressures) used in our experiments.

Data in Figure 4a show that the CO oxidation rates, measured at temperatures between 100 and 150 °C (no light illumination), were similar for the four catalysts with different Ag loadings. This consistency in the measured rates is reassuring since it indicates that the reactor is operating in a kinetic regime, wherein the observed rate is not influenced by mass transfer limitations, even at higher weight loadings. Data in Figure 4b show the photorates on different catalysts plotted as a function of thermal rates. The photorate was calculated by subtracting the reaction rate measured under thermal conditions (plotted in Figure 4a) from the respective rates measured under photothermal conditions at the same power supply to the external heater. The data show that the photorates normalized per gram of Ag are very similar for catalyst loadings of 1.5, 3, and 6 wt %, suggesting that any collective nanoparticle interactions (collective effects) do not appear to emerge for these low-loading samples. By "collective effects", we are referring to any process that changes the reaction rate per mass of the material as the loading of Ag nanoparticles changes. We note that at higher loading we observe enhanced levels of particle clustering. One example of these collective processes can be collective heating, where due to the nanoparticles' proximity to one another, the particles mutually heat each other. Alternatively, this proximity can cause an increase in the rates of electronic excitations that take place due to elevated local fields between the nanoparticles. In other words, the data suggest that each nanoparticle operates relatively independently under illumination for catalysts of low loading. On the other hand, for the 12 wt % catalyst, we find

that the photorates normalized per gram of Ag exceed those of the lower-loaded catalysts. The data show that at this higher loading collective effects intensify, giving an additional boost to the reaction rates. We hypothesized that at these higher loadings, the Ag clustering could lead to more pronounced collective effects, which can drive up the reaction rate per gram of Ag under illumination. This hypothesis is consistent with previous findings that showed collective heating tends to be prominent at high nanoparticle densities, that at low intensities the effect of photothermal heating can be negligible, and that the plasmonic rate enhancement observed in these systems must be attributed to nonthermal processes (charge-carrier-driven chemistry). A similar trend in the enhancement factor $(r_{\text{photothermal}}/r_{\text{thermal}})$ as a function of thermal rate is provided in Figure 4c.

To further explore the relationship between nanoparticle clustering, equilibrium heating, and the observed photorates, we embedded thermocouples in the catalyst bed to measure the temperature increase for the four catalysts under specific reaction conditions. Before illuminating the catalysts, we set up an external thermal setpoint of 100 °C (this is the setpoint at which the corresponding thermal measurements were performed). We applied the same heater power when performing corresponding photocatalytic measurements. We used thin PTFE-wrapped thermocouples placed as close to the light source as possible (at the exterior wall of the annular region) and as close to the heater as possible (at the interior wall of the annular region) to measure the thermal and photothermal temperature gradients for each case. An illustration of this setup is provided in the inset of Figure 5a. As noted above, we found that the PTFE-wrapped thermocouple does tend to overestimate the temperature reading of the catalyst under illumination, by ~5-6 °C, when positioned near the light source. We nonetheless report the asmeasured temperature readings from this thermocouple without any additional corrections to avoid any possibility of underestimating the macroscopic (equilibrium) photothermal temperatures.

Data in Figure 5a show measured temperature increases for each catalyst under illumination for the two different regions of

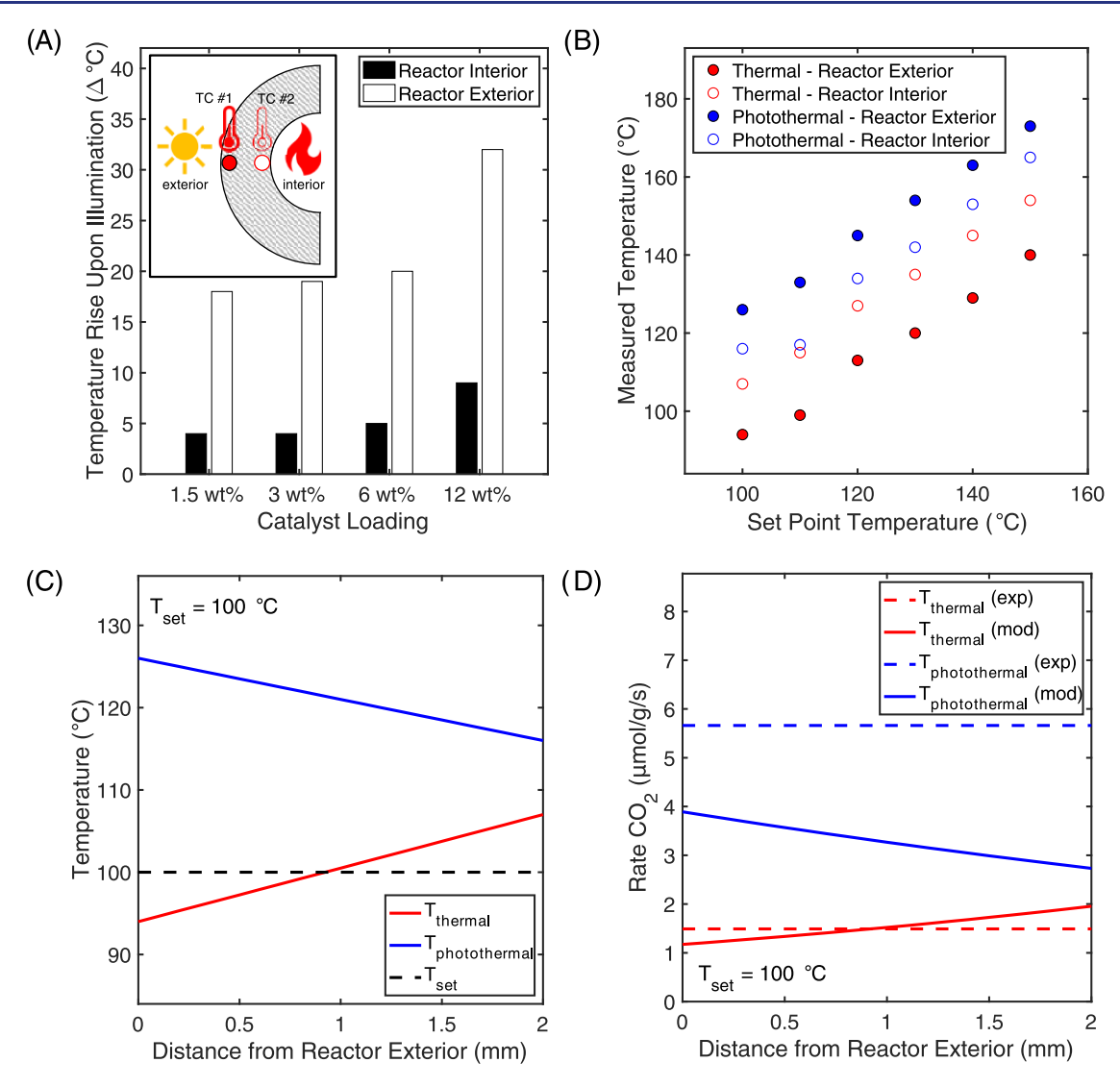


Figure 5. Spatial temperature and rate measurements in the annular reactor. (A) Temperature increase measured under illumination for all four catalyst samples at the reactor interior (closest to the heater, black bars) and exterior (closest to the light source, white bars) under CO oxidation conditions. The inset figure shows a sketch of the relative thermocouple positions at the interior and exterior of the catalyst bed; (B) experimentally measured temperatures under thermal (red) and photothermal (blue) conditions as a function of thermal setpoint for the 12 wt % catalyst; (C) thermal and photothermal temperature profiles in the annular reactor; the photothermal temperature profile suggests that most of the heating takes place closest to the light source; (D) experimentally measured thermal (red dashed line) and photothermal (blue dashed line) reaction rates compared to thermal (solid red line) and photothermal (solid blue line) Arrhenius rates, modeled in the reactor as a function of distance, assuming that the reactants are at the measured equilibrium temperatures.

the reactor, with the heater kept at the power setpoint identical to that required for the thermal measurements at 100 °C. As expected, the extent of measured heating under illumination is more significant directly under the light source (reactor exterior) compared to far from the light source (reactor interior). The data show that there were relatively similar temperature increases for the 1.5, 3, and 6 wt % cases, with only small changes in temperature observed with increasing loading. We believe that the gas flowing throughout the reactor convectively cools these catalysts, limiting the extent of temperature increase as measured by the thermocouple under light. On the other hand, our measurements also indicate that the 12 wt % loading case exhibits a significantly larger increase in temperature under light. This is consistent with a regime in which highly clustered, high-density nanoparticle catalysts yield stronger collective effects, including

equilibrium heating, that can be observed at the macroscopic level.

We performed identical measurements, as in Figure 5a, measuring the thermal and photothermal temperature profiles in the annular reactor for thermal setpoint temperatures ranging between 100 and 150 °C (i.e., the catalyst temperature controlled by the external heater under thermal conditions in the absence of illumination). In these measurements, we focused on two catalyst loadings (the 6 and 12 wt % Ag loadings). The data in Figure 5b show the measured temperatures recorded at the interior and exterior annular reactor positions under thermal conditions (red) and photothermal conditions (blue) for the 12 wt % catalyst. The corresponding data for the 6 wt % catalyst are included in Figure S10 and follow a similar trend. If we assume a linear temperature gradient between the two positions in the reactor—this assumption is reasonable since the reactor has

a very short radial length of ~2 mm²⁴—we can obtain estimated temperature profiles across the reactor. One of these temperature profiles is shown in Figure 5c for the 12 wt % catalyst at a thermal setpoint of 100 °C. The Supporting Information provides the corresponding temperature profiles at different thermal setpoints for the 6 wt % catalyst (Figure S11) and the 12 wt % catalyst (Figure S13).

We next analyzed if the extent of the measured illuminationinduced equilibrium heating could describe the plasmonic rate enhancements that we experimentally measured (Figure 4) under illumination for the CO oxidation reaction. Using the Arrhenius rate constant measured in the temperature-dependent thermal studies (data provided in Figure 4a) and the temperature profiles in Figures 5c, S11, and S13, we calculated the anticipated photothermal rate as a function of the position in the reactor for the 6 and 12 wt % catalysts assuming that the photothermal reaction is driven solely by the illuminationinduced equilibrium temperature enhancement. Figure 5d shows the calculated Arrhenius reaction rates under thermal and photothermal operation for the 12 wt % catalyst at a thermal setpoint of 100 °C. The Supporting Information provides the corresponding data for the 6 wt % catalyst (Figure \$12) and supplementary data for the 12 wt % catalyst at other thermal setpoint temperatures (Figure S14).

The data in Figure 5d show that the predicted Arrhenius photothermal rate (solid blue line) is well below the photothermal rate experimentally measured when we study the catalysts under illumination (dashed blue line). This is very different compared to the thermal measurements (no illumination), for which, as expected, the measured temperatures accurately predict the magnitude of the reaction rates. The data in Figure 5d clearly show that steady-state equilibrium heating cannot completely capture the behavior of the systems and that localized effects need to be invoked. Identical observations were made for the case of the 6 wt % catalyst, with the data provided in the Supporting Information.

A comparison of the data in Figures 5d, S12, and S14 shows that as the catalyst loading changes from 6 to 12 wt %, the total photorate per gram of Ag attributed to these non-Arrhenius effects also increases. We attribute the increase to a few potential factors. For instance, dense regions of highly clustered nanoparticles could give rise to the emergence of stronger localized nonthermal mechanisms that are confined near the clusters and spaces between adjacent nanoparticles. These may involve the elevated electric fields between nanoparticles that lead to increased local charge-carrier-driven processes at the adsorbate/metal interfaces. 4,5,14 Charge carriers can participate in the reaction via their excitation by either the so-called indirect or direct charge-transfer mechanisms. In the indirect mechanism, light excites electrons or holes within the metal, which then transiently populate the electronic states of an adsorbate (reactant). The adsorbate is temporarily moved to a transient negative ion state, resulting in the activation of chemical bonds and ultimately the chemical transformation of the adsorbate. In the direct mechanism, also referred to as chemical interface damping, the decay of the high fields at the interface between the nanoparticle and adsorbate results in direct charge-carrier excitation at the adsorbate-metal interface, again facilitating a chemical transformation of the adsorbate.8 Furthermore, we and others have previously demonstrated that nonthermal charge-carrier-driven processes can become more efficient at elevated temperatures due to the temperature-dependent coupling of electronic and

vibrational excitations of molecules on the surface of plasmonic nanoparticles. 4,19,31,45 Ultimately, the data clearly show that while photothermal equilibrium heating may play some role in observed plasmonic rate enhancements under conditions of broadband continuous illumination, there are significant additional contributions that cannot be described by the equilibrium heating of the catalyst bed.

CONCLUSIONS

In conclusion, we designed an annular photoreactor that allowed us to accurately measure the steady-state equilibrium temperature under reaction conditions in different parts of the catalyst bed while concurrently allowing us to measure the reaction rates in the kinetic regime. Our measurements of the CO oxidation rates across four different weight loadings of plasmonic Ag/α - Al_2O_3 catalysts suggest that under the studied illumination conditions, collective effects arising when plasmonic Ag nanoparticles (~64 nm diameter) interact with neighboring nanoparticles induce a significant change in the reaction rate for Ag/α - Al_2O_3 loadings above 6 wt % (i.e., clusters of nanoparticles begin to exceed 10 particles condensed within an $\sim 0.15 \ \mu \text{m}^2$ imaged region). Lower weight loadings do not demonstrate any loading-dependent collective contributions to measured reaction rates under illumination. In other words, for low Ag loading samples, the measured photorates per catalyst surface area are similar, suggesting that each particle behaves relatively independently of one another. We also observed that the equilibrium heating of the catalyst cannot fully explain the illumination-induced plasmonic rate enhancements. This holds true even for dense and highly clustered loadings of Ag nanoparticles, where equilibrium heating becomes more significant. Based on the analysis, we propose that highly localized effects play a critical role in driving LSPR-induced chemical reactions. These effects may consist of plasmon-induced activation of adsorbates (reactants) via electronic excitation of the reactant or photothermal heating of adsorbates that remains highly localized to the individual nanoparticles.

ASSOCIATED CONTENT

Supporting Information

The Supporting Information is available free of charge at https://pubs.acs.org/doi/10.1021/jacs.2c08561.

Details of the reactor design, nanoparticle and catalyst syntheses and characterization, reaction conversions and quantum yields, thermocouple modification, quantification of clustering, light source spectrum, supplementary experimental temperature and rate data, and additional references (PDF)

AUTHOR INFORMATION

Corresponding Author

Suljo Linic – Department of Chemical Engineering, University of Michigan, Ann Arbor, Michigan 48109, United States; Catalysis Science and Technology Institute, University of Michigan, Ann Arbor, Michigan 48109, United States; orcid.org/0000-0003-2153-6755; Email: linic@ umich.edu

Author

Rachel C. Elias - Department of Chemical Engineering, University of Michigan, Ann Arbor, Michigan 48109, United States; Catalysis Science and Technology Institute, University of Michigan, Ann Arbor, Michigan 48109, United States; orcid.org/0000-0002-1085-8372

Complete contact information is available at: https://pubs.acs.org/10.1021/jacs.2c08561

Notes

The authors declare no competing financial interest.

ACKNOWLEDGMENTS

The work presented in this document was supported by the National Science Foundation (NSF) (CHE-1800197). Secondary support was provided by the U.S. Department of Energy, Office of Science, Office of Basic Energy Sciences (DE-SC0021362) (analysis of optical interactions of materials with light), and the Office of Basic Energy Science, Division of Chemical Sciences (DE-SC0021008) (material synthesis). The electron microscopy measurements were supported by the University of Michigan College of Engineering.

REFERENCES

- (1) Willets, K. A.; Van Duyne, R. P. Localized Surface Plasmon Resonance Spectroscopy and Sensing. *Annu. Rev. Phys. Chem.* **2007**, 58, 267–297.
- (2) Kelly, K. L.; Coronado, E.; Zhao, L. L.; Schatz, G. C. The Optical Properties of Metal Nanoparticles: The Influence of Size, Shape, and Dielectric Environment. J. Phys. Chem. B 2003, 107, 668–677.
- (3) Schuller, J. A.; Barnard, E. S.; Cai, W.; Jun, Y. C.; White, J. S.; Brongersma, M. L. Plasmonics for Extreme Light Concentration and Manipulation. *Nat. Mater.* **2010**, *9*, 193–204.
- (4) Linic, S.; Christopher, P.; Ingram, D. B. Plasmonic-Metal Nanostructures for Efficient Conversion of Solar to Chemical Energy. *Nat. Mater.* **2011**, *10*, 911–921.
- (5) Linic, S.; Aslam, U.; Boerigter, C.; Morabito, M. Photochemical Transformations on Plasmonic Metal Nanoparticles. *Nat. Mater.* **2015**, *14*, 567–576.
- (6) Robatjazi, H.; Yuan, L.; Yuan, Y.; Halas, N. J. Heterogeneous Plasmonic Photocatalysis: Light-Driven Chemical Reactions Introduce a New Approach to Industrially-Relevant Chemistry. In *Emerging Trends in Chemical Applications of Lasers*, ACS Symposium Series; American Chemical Society, 2021; Vol. 1398, pp 363–387.
- (7) Aslam, U.; Rao, V. G.; Chavez, S.; Linic, S. Catalytic Conversion of Solar to Chemical Energy on Plasmonic Metal Nanostructures. *Nat. Catal.* **2018**, *1*, 656–665.
- (8) Seemala, B.; Therrien, A. J.; Lou, M.; Li, K.; Finzel, J. P.; Qi, J.; Nordlander, P.; Christopher, P. Plasmon-Mediated Catalytic O2 Dissociation on Ag Nanostructures: Hot Electrons or near Fields? *ACS Energy Lett.* **2019**, *4*, 1803–1809.
- (9) Christopher, P.; Xin, H.; Linic, S. Visible-Light-Enhanced Catalytic Oxidation Reactions on Plasmonic Silver Nanostructures. *Nat. Chem.* **2011**, *3*, 467–472.
- (10) Mukherjee, S.; Libisch, F.; Large, N.; Neumann, O.; Brown, L. V.; Cheng, J.; Lassiter, J. B.; Carter, E. A.; Nordlander, P.; Halas, N. J. Hot Electrons Do the Impossible: Plasmon-Induced Dissociation of H2 on Au. *Nano Lett.* **2013**, *13*, 240–247.
- (11) Brongersma, M. L.; Halas, N. J.; Nordlander, P. Plasmon-Induced Hot Carrier Science and Technology. *Nat. Nanotechnol.* **2015**, *10*, 25–34.
- (12) Marimuthu, A.; Zhang, J.; Linic, S. Tuning Selectivity in Propylene Epoxidation by Plasmon Mediated Photo-Switching of Cu Oxidation State. *Science* **2013**, *339*, 1590–1593.
- (13) Mukherjee, S.; Zhou, L.; Goodman, A. M.; Large, N.; Ayala-Orozco, C.; Zhang, Y.; Nordlander, P.; Halas, N. J. Hot-Electron-Induced Dissociation of H2 on Gold Nanoparticles Supported on SiO2. J. Am. Chem. Soc. 2014, 136, 64–67.

- (14) Christopher, P.; Xin, H.; Marimuthu, A.; Linic, S. Singular Characteristics and Unique Chemical Bond Activation Mechanisms of Photocatalytic Reactions on Plasmonic Nanostructures. *Nat. Mater.* **2012**, *11*, 1044–1050.
- (15) Li, S.; Huang, H.; Shao, L.; Wang, J. How to Utilize Excited Plasmon Energy Efficiently. ACS Nano 2021, 15, 10759–10768.
- (16) Hamans, R. F.; Parente, M.; Baldi, A. Super-Resolution Mapping of a Chemical Reaction Driven by Plasmonic near-Fields. *Nano Lett.* **2021**, 21, 2149–2155.
- (17) Aslam, U.; Chavez, S.; Linic, S. Controlling Energy Flow in Multimetallic Nanostructures for Plasmonic Catalysis. *Nat. Nanotechnol.* **2017**, *12*, 1000–1005.
- (18) Boerigter, C.; Campana, R.; Morabito, M.; Linic, S. Evidence and Implications of Direct Charge Excitation as the Dominant Mechanism in Plasmon-Mediated Photocatalysis. *Nat. Commun.* **2016**, *7*, No. 10545.
- (19) Boerigter, C.; Aslam, U.; Linic, S. Mechanism of Charge Transfer from Plasmonic Nanostructures to Chemically Attached Materials. ACS Nano 2016, 10, 6108–6115.
- (20) Kamarudheen, R.; Castellanos, G. W.; Kamp, L. P. J.; Clercx, H. J. H.; Baldi, A. Quantifying Photothermal and Hot Charge Carrier Effects in Plasmon-Driven Nanoparticle Syntheses. *ACS Nano* **2018**, *12*, 8447–8455.
- (21) Mascaretti, L.; Naldoni, A. Hot Electron and Thermal Effects in Plasmonic Photocatalysis. *J. Appl. Phys.* **2020**, *128*, No. 041101.
- (22) Rodio, M.; Graf, M.; Schulz, F.; Mueller, N. S.; Eich, M.; Lange, H. Experimental Evidence for Nonthermal Contributions to Plasmon-Enhanced Electrochemical Oxidation Reactions. *ACS Catal.* **2020**, *10*, 2345–2353.
- (23) Yu, Y.; Sundaresan, V.; Willets, K. A. Hot Carriers versus Thermal Effects: Resolving the Enhancement Mechanisms for Plasmon-Mediated Photoelectrochemical Reactions. *J. Phys. Chem.* C 2018, 122, 5040–5048.
- (24) Zhang, X.; Li, X.; Reish, M. E.; Zhang, D.; Su, N. Q.; Gutiérrez, Y.; Moreno, F.; Yang, W.; Everitt, H. O.; Liu, J. Plasmon-Enhanced Catalysis: Distinguishing Thermal and Nonthermal Effects. *Nano Lett.* **2018**, *18*, 1714–1723.
- (25) Kamarudheen, R.; Aalbers, G. J. W.; Hamans, R. F.; Kamp, L. P. J.; Baldi, A. Distinguishing among All Possible Activation Mechanisms of a Plasmon-Driven Chemical Reaction. *ACS Energy Lett.* **2020**, *5*, 2605–2613.
- (26) Cortés, E.; Besteiro, L. V.; Alabastri, A.; Baldi, A.; Tagliabue, G.; Demetriadou, A.; Narang, P. Challenges in Plasmonic Catalysis. *ACS Nano* **2020**, *14*, 16202–16219.
- (27) Baffou, G.; Cichos, F.; Quidant, R. Applications and Challenges of Thermoplasmonics. *Nat. Mater.* **2020**, *19*, 946–958.
- (28) Cortés, E.; Grzeschik, R.; Maier, S. A.; Schlücker, S. Experimental Characterization Techniques for Plasmon-Assisted Chemistry. *Nat. Rev. Chem.* **2022**, *6*, 259–274.
- (29) Linic, S.; Chavez, S.; Elias, R. Flow and Extraction of Energy and Charge Carriers in Hybrid Plasmonic Nanostructures. *Nat. Mater.* **2021**, 20, 916–924.
- (30) Song, C.; Wang, Z.; Yin, Z.; Xiao, D.; Ma, D. Principles and Applications of Photothermal Catalysis. *Chem. Catal.* **2022**, *2*, 52–83.
- (31) Kale, M. J.; Avanesian, T.; Christopher, P. Direct Photocatalysis by Plasmonic Nanostructures. *ACS Catal.* **2014**, *4*, 116–128.
- (32) Bonn, M.; Funk, S.; Hess, C.; Denzler, D. N.; Stampfl, C.; Scheffler, M.; Wolf, M.; Ertl, G. Phonon-versus Electron-Mediated Desorption and Oxidation of CO on Ru(0001). *Science* **1999**, 285, 1042–1045.
- (33) Li, X.; Zhang, X.; Everitt, H. O.; Liu, J. Light-Induced Thermal Gradients in Ruthenium Catalysts Significantly Enhance Ammonia Production. *Nano Lett.* **2019**, *19*, 1706–1711.
- (34) Baffou, G.; Bordacchini, I.; Baldi, A.; Quidant, R. Simple Experimental Procedures to Distinguish Photothermal from Hot-Carrier Processes in Plasmonics. *Light: Sci. Appl.* **2020**, *9*, 108.
- (35) Zhou, L.; Swearer, D. F.; Zhang, C.; Robatjazi, H.; Zhao, H.; Henderson, L.; Dong, L.; Christopher, P.; Carter, E. A.; Nordlander,

- P.; Halas, N. J. Quantifying Hot Carrier and Thermal Contributions in Plasmonic Photocatalysis. Science 2018, 362, 69-72
- (36) Robatjazi, H.; Zhao, H.; Swearer, D. F.; Hogan, N. J.; Zhou, L.; Alabastri, A.; McClain, M. J.; Nordlander, P.; Halas, N. J. Plasmon-Induced Selective Carbon Dioxide Conversion on Earth-Abundant Aluminum-Cuprous Oxide Antenna-Reactor Nanoparticles. Nat. Commun. 2017, 8, No. 27.
- (37) Zhou, L.; Martirez, J. M. P.; Finzel, J.; Zhang, C.; Swearer, D. F.; Tian, S.; Robatjazi, H.; Lou, M.; Dong, L.; Henderson, L.; Christopher, P.; Carter, E. A.; Nordlander, P.; Halas, N. J. Light-Driven Methane Dry Reforming with Single Atomic Site Antenna-Reactor Plasmonic Photocatalysts. Nat. Energy 2020, 5, 61-70.
- (38) Yablonsky, G.; Marin, G. B.; Fushimi, R. R. Kinetic Measurements in Heterogeneous Catalysis; Wiley: Hoboken, NJ, 2021.
- (39) Christopher, P.; Linic, S. Shape- and Size-Specific Chemistry of Ag Nanostructures in Catalytic Ethylene Epoxidation. ChemCatChem 2010, 2, 78-83.
- (40) Aslam, U.; Linic, S. Kinetic Trapping of Immiscible Metal Atoms into Bimetallic Nanoparticles through Plasmonic Visible Light-Mediated Reduction of a Bimetallic Oxide Precursor: Case Study of Ag-Pt Nanoparticle Synthesis. Chem. Mater. 2016, 28, 8289-8295.
- (41) Dix, S. T.; Linic, S. In-Operando Surface-Sensitive Probing of Electrochemical Reactions on Nanoparticle Electrocatalysts: Spectroscopic Characterization of Reaction Intermediates and Elementary Steps of Oxygen Reduction Reaction on Pt. J. Catal. 2021, 396, 32-
- (42) Perera, I. U.; Narendran, N.; Liu, Y. Accurate Measurement of LED Lens Surface Temperature. In LED-based Illumination Systems; International Society for Optics and Photonics, 2013; Vol. 8835, p
- (43) Baffou, G.; Berto, P.; Bermúdez Ureña, E.; Quidant, R.; Monneret, S.; Polleux, J.; Rigneault, H. Photoinduced Heating of Nanoparticle Arrays. ACS Nano 2013, 7, 6478-6488.
- (44) Zhan, C.; Wang, Q.-X.; Yi, J.; Chen, L.; Wu, D.-Y.; Wang, Y.; Xie, Z.-X.; Moskovits, M.; Tian, Z.-Q. Plasmonic Nanoreactors Regulating Selective Oxidation by Energetic Electrons and Nanoconfined Thermal Fields. Sci. Adv. 2021, 7, No. eabf0962.
- (45) Olsen, T.; Gavnholt, J.; Schiøtz, J. Hot-Electron-Mediated Desorption Rates Calculated from Excited-State Potential Energy Surfaces. Phys. Rev. B 2009, 79, No. 035403.

□ Recommended by ACS

Can Light Alter the Yield of Plasmon-Driven Reactions on **Gold and Gold-Palladium Nanoplates?**

Zhandong Li and Dmitry Kurouski

SEPTEMBER 19 2022

NANO I FTTERS

READ 2

Plasmon-Assisted Direct Interfacial Charge Transfer Enables Molecular Photodissociation on Metal Surfaces

Taha Salavati-fard and Bin Wang

OCTOBER 10, 2022

ACS CATALYSIS

READ **C**

Plasmonic Photocatalysis with Chemically and Spatially Specific Antenna-Dual Reactor Complexes

Lin Yuan, Naomi J. Halas, et al.

OCTOBER 06, 2022

ACS NANO

READ **C**

Nanofluidic Trapping of Faceted Colloidal Nanocrystals for **Parallel Single-Particle Catalysis**

Sune Levin, Christoph Langhammer, et al.

SEPTEMBER 02, 2022

ACS NANO

READ 2

Get More Suggestions >